

Resolving the enigmatic solar wind disappearance event of 11 May 1999

P. Janardhan

Astronomy and Astrophysics Division, Physical Research Laboratory, Ahmedabad, India

K. Fujiki, M. Kojima, and M. Tokumaru

Solar-Terrestrial Environment Laboratory, Nagoya University, Aichi, Japan

K. Hakamada

Department of Natural Science and Mathematics, Chubu University, Kasugai, Japan

Received 12 April 2004; revised 14 March 2005; accepted 7 April 2005; published 3 August 2005.

[1] On 11 and 12 May 1999, the Earth was engulfed by an unusually low-density ($<1 \text{ cm}^{-3}$) and low-velocity ($<350 \text{ km s}^{-1}$) solar wind for a period of over 1 day. Extensive studies of this unusual event that occurred during Carrington rotation 1949 (CR1949), using both ground-based and space-based in situ observations, have not as yet been able to identify the cause or the solar source of this event. Using solar wind velocity measurements from the four-station IPS observatory of the Solar-Terrestrial Environment Laboratory (STEL), Toyokawa, Japan, we investigate the structure of the solar wind in May 1999 during CR1949. IPS observations from STEL were used to make tomographic velocity maps to identify and delineate the extent and morphology of the stable solar wind flows during CR1949 in the vicinity of the Earth. Combined with in situ measurements of the interplanetary magnetic field (IMF), potential field computations of the solar magnetic fields in the period, and He I 10830Å observations of coronal hole boundaries during CR1949, we have identified the source region of the unusual flows and have shown that the flow responsible for the “disappearance event” was a stable unipolar flow originating in the vicinity of a large midlatitude active region AR8525, located at $\sim 18^\circ\text{N}$ and between heliographic longitudes 280° and 300° . Earlier workers have speculated that such events may be caused by the large-scale restructuring of the solar magnetic field at the maximum of each solar cycle. However, by identifying the solar source and nature of this event, we believe that at least in this particular case, the association with global, large-scale solar phenomena like the periodic 11-year solar polar field reversal is most likely to be coincidental.

Citation: Janardhan, P., K. Fujiki, M. Kojima, M. Tokumaru, and K. Hakamada (2005), Resolving the enigmatic solar wind disappearance event of 11 May 1999, *J. Geophys. Res.*, *110*, A08101, doi:10.1029/2004JA010535.

1. Introduction

[2] For a steady state flow of solar wind and at the Sun-Earth distance of 1 astronomical unit (AU), densities and velocities are known to be inversely correlated with lower velocities having higher than average densities and vice versa. However, on 11 and 12 May 1999, the Earth was engulfed by an unusually low-density ($<0.1 \text{ cm}^{-3}$) and low-velocity ($<350 \text{ km s}^{-1}$) solar wind. This was a unique low-velocity, low-density flow which spacecraft observations have shown lasted more than 24 hours. One consequence of this extremely tenuous solar wind was a spectacular expansion of the Earth’s magnetosphere and bow shock. The expanding bow shock was observed by several spacecraft and reached record upstream distances of nearly 60 Earth radii, the lunar orbit. The event was so dramatic that it has come to be known as “the solar wind disappearance event.” Extensive studies of

the event have been reported using both space-based and ground-based observations [Crooker *et al.*, 2000; Farrugia *et al.*, 2000; Richardson *et al.*, 2000; Usmanov *et al.*, 2000; Vats *et al.*, 2001; Balasubramanian *et al.*, 2003], but none have been able to explain the cause or locate the solar source of the event. For unsteady flow, it is known that strong transient events produce, at first, strong high-speed compressed flow behind a strong shock. This behavior can then be followed by a deep expansion to low densities when the speed dramatically decreases. Such a situation did not occur during this instance as will be shown later. The event has therefore remained an enigma and has raised questions about how the solar wind could be turned off for a period of 24 hours or more.

2. Interplanetary Scintillation Observations of the Solar Wind

[3] Interplanetary scintillation (IPS) observations of compact extragalactic radio sources provides one with an

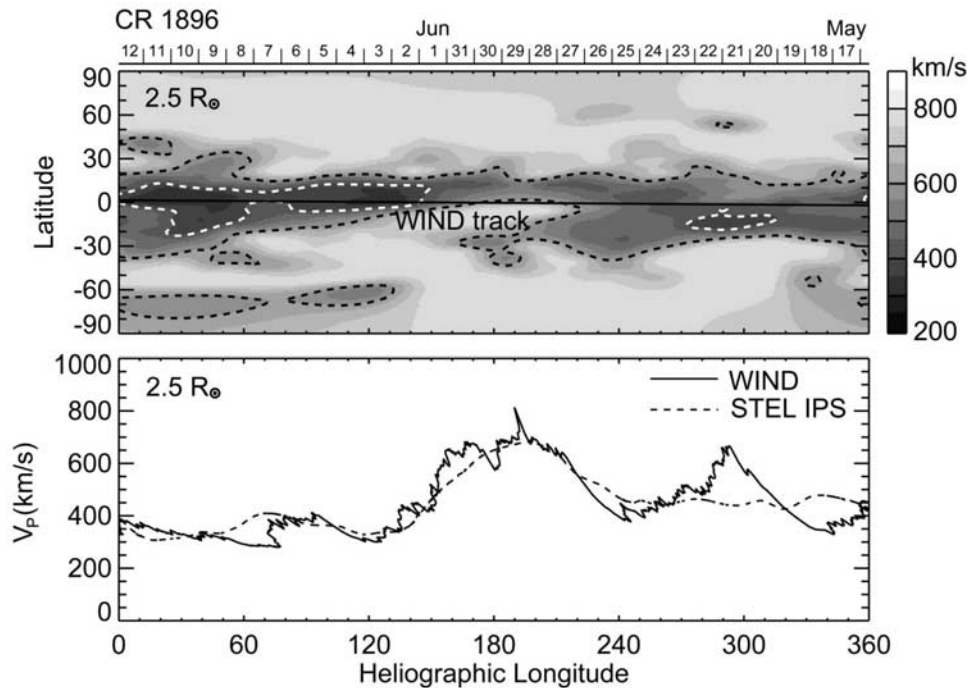


Figure 1. (top) A tomographic synoptic velocity map projected on to the source surface at $2.5 R_{\odot}$ for CR1896 in May–June 1995, obtained using STEL IPS data. The dashed white and black lines demarcate the boundaries of the low-velocity flows and polar coronal hole boundaries respectively. Dates of CMP are indicated at the top of the map, while the path of the Wind spacecraft is indicated by a thick line along the equator. (bottom) Wind in situ measurements of proton velocities as a function of heliographic longitude (solid line) that have been projected back to $2.5 R_{\odot}$ along Archimedean spirals and IPS velocities (dashed line) extracted along the path of the Wind spacecraft from the IPS synoptic map in the top part.

efficient and cost-effective ground-based method for studying the large-scale properties of the solar wind plasma. The main parameters measurable by IPS are the solar wind velocities and the root mean square deviation in the electron density distribution of the density irregularities in the solar wind. Both these parameters represent weighted averages along the line of sight (LOS) to the compact extragalactic radio source that is under observation. Thus each IPS observation probes the interplanetary medium at a particular heliolatitude and distance from the Sun, depending upon the observed radio source position and its solar elongation (ϵ), the angle between the LOS to the source, and the Sun–Earth line.

[4] At an observing frequency of 327 MHz, the operating frequency of the dedicated four-station IPS observatory at STEL, Japan, the coverage in ϵ is $10^{\circ} \leq \epsilon \leq 60^{\circ}$. This corresponds to $0.2 \text{ AU} \leq r \leq 0.9 \text{ AU}$ or $40 R_{\odot} \leq r \leq 190 R_{\odot}$, where r is the distance between the Sun and the LOS to the source and R_{\odot} is the solar radius. Thus regular IPS observations of a large number of compact, spatially well distributed radio sources can not only be used to get a large-scale picture of the velocity structure and density fluctuations prevailing in the solar wind but can also be used to track traveling interplanetary disturbances on a day-to-day basis [Janardhan *et al.*, 1996].

[5] Regular and systematic IPS observations of the solar wind in the inner heliosphere at 327 MHz have been carried out at STEL, Japan for many decades now. Using these

observations, estimates of solar wind velocities are derived by the method of triangulation [Kakinuma and Kojima, 1984] by using a cross-correlation analysis between the six pairs of baselines available with the four-station system. In recent years a tomographic technique has been developed and applied to STEL solar wind data that overcomes the LOS integration effects that are inherent in the IPS observations [Jackson *et al.*, 1998; Kojima *et al.*, 1998; Asai *et al.*, 1998]. The tomographic technique obtains a best fit to IPS observations using an iterative method and a three-dimensional model of the solar wind [Jackson *et al.*, 1998]. One can thus obtain LOS integrated model IPS observations that match the actual IPS observations as nearly as possible. The resolution of the three-dimensional structure is, however, limited by the amount of data used and the inherent noise and therefore the analysis is usually presented as Carrington synoptic velocity maps, each made using approximately 600 observations of velocity obtained over a period of one full Carrington rotation and projected to a fixed heliocentric distance. This distance can be the solar surface, the source surface at $2.5 R_{\odot}$ or 1 AU. The IPS velocities can then be mapped from the reference surface in the model by projecting it radially outward (or inward) using a constant velocity. Synoptic velocity maps created by this technique are therefore less biased and represent more realistically the large-scale structure of the solar wind.

[6] The uppermost part of Figure 1 shows an example of a tomographic synoptic velocity map obtain using IPS

measurements from STEL during a straightforward and well-understood situation during solar minimum. We will later discuss the situation during the period of interest in May 1999. The synoptic map shows solar wind velocities as a function of heliographic longitude and latitude for Carrington rotation 1896 (CR1896) in May–June 1995. The path of the Wind spacecraft is indicated by a thick line along the equator. The map uses all observations of velocity obtained over a period of 1 month during CR1896 with care being taken to ensure that data affected by terrestrial interference were first removed. The dashed black lines on the map demarcate the polar coronal hole boundaries, while the dashed white lines demarcate the boundaries of the low-velocity flows ($<400 \text{ km s}^{-1}$). The velocities are projected on the source surface at a distance of $2.5 R_{\odot}$. The dates of central meridian passage (CMP) are indicated at the top of the map. The bottom part of Figure 1 shows Wind in situ measurements of velocity (black solid line) after every individual velocity measurement has been projected back from 1 AU to the source surface along Archimedean spirals. The black dashed curve in Figure 1 represents velocities extracted along the equator from the synoptic map in the upper part. It can be seen from Figure 1 that the velocities obtained from the tomographic synoptic map match the Wind spacecraft observations extremely well, considering that the comparison is being made between hourly values of in situ measurements and model derived IPS velocities obtained from IPS observations carried out over one full Carrington rotation. The tomographic technique can be thus used to reliably reproduce and study the large-scale, stable, and long-lasting solar wind flows. It should be borne in mind, however, that unlike the solar minimum phase discussed here, the solar maximum phase shows rapid changes in structure due mainly because of transient events that take place over a timescale of days. Thus tomographic velocity maps at solar maximum, as in CR1949 during May 1999 which will be discussed later, will show only the average large-scale and stable structure of the solar wind, while transient features will not be seen. Also, the errors in the constant velocity traceback method used above to project Wind velocities back to $2.5 R_{\odot}$ will depend upon the nature of the solar wind flow. More detailed discussions on the reliability of IPS tomographic mapping technique can be found in the work of *Kojima et al.* [1998, 1999].

3. Observations

3.1. In Situ Measurements

[7] The first and second parts of Figure 2 show ACE in situ measurements of proton density and velocities during our time of interest in May 1999. The magnitude of the interplanetary magnetic field (IMF) and the azimuthal direction of the magnetic field in the ecliptic plane are shown in the third and fourth parts. The direction of the magnetic field is computed from measurements of B_x and B_y , the X and Y components of the IMF in Geocentric Solar Ecliptic (GSE) coordinates. It is important to note that the magnitude of the magnetic field shows hardly any fluctuations during day of year (DOY) 131 and the direction of the field remains constant. This is in contrast to other days when the direction of the field shows large and rapid changes (c.f. DOY 138). The low variance in the magnitude

of the magnetic field and the lack of change in the actual direction of the magnetic field indicate that the solar wind flow during 11 May 1999 (DOY 131) was stable and unipolar. For a radial flow of solar wind at a velocity of 430 km s^{-1} , the tangent to an Archimedean spiral at 1 AU will make an angle of 45° with the radial vector from the Sun. The deviation of this angle from the expected value, for the measured velocities, is shown in the lowermost part of Figure 2 and it can be seen that the solar wind at 1 AU on DOY 131 was characterized by highly nonradial flows. From the uppermost part of Figure 2 it can be seen that the densities first began dropping on DOY 130. Figure 3 shows the relation between density and azimuthal or V_y component of velocity (in GSE coordinates) observed during DOY 130 and 131. It can be seen that the westward flow deviation increases as the density decreases. This nonradial flow in the azimuthal direction will be discussed in detail later. The two parallel lines running vertically across all parts of Figure 2 demarcate the date 11 May 1999 corresponding to DOY 131. The two dashed vertical parallel lines in the fifth part of Figure 2 are drawn at DOY 129.5 and DOY 134. The reason for showing these lines in Figure 2 as also the origin of the nonradial flow will be discussed later.

[8] In situ observations of the solar wind have shown that transitions from a slow solar wind flow to a high-speed stream or vice versa show up as stream interfaces characterized by abrupt and large changes in density and velocity [*Burlaga, 1974; Gosling et al., 1978*]. From the first and second parts of Figure 2, we can see that apart from DOY 125 when the velocity and density show a sudden change, the solar wind flow between DOY 120–125 and DOY 126–131 is smoothly varying with no large and abrupt jumps in densities and velocities. There is thus no evidence of clear stream-stream interactions or stream interfaces in the ACE data that could introduce large errors in the determination of source locations on the Sun.

3.2. Ground-Based IPS Observations

[9] The uppermost part of Figure 4 shows a tomographic synoptic velocity map for Carrington rotation 1949 (CR1949) in May 1999, obtained using IPS data from STEL. Filled black regions on the map indicate data gaps. Dashed white lines demarcate the boundaries of the low-velocity flows ($<400 \text{ km s}^{-1}$), while the dashed black lines demarcate the polar coronal hole boundaries. The velocities are projected on the source surface at $2.5 R_{\odot}$. Dates of CMP are indicated at the bottom of the map and the path of the ACE spacecraft is shown by a thick line along the equator. It can be seen from Figure 4 (top) that the solar wind during CR1949 was dominated by large, stable, low-velocity flows that occupied most of the inner heliosphere. The two small high-velocity regions lying between 280° and 340° and north and south of the equator, respectively, originate from equatorward extensions of the large polar coronal holes located beyond 60° latitudes in both hemispheres.

[10] The second part of Figure 4 uses the measured ACE velocities at 1 AU ($215 R_{\odot}$) that are shown in Figure 2 (second part) and traces each one back to the source surface at $2.5 R_{\odot}$ using constant velocities along corresponding Archimedean spirals. Parallel solid lines running vertically across both the parts of Figure 4 bracket the DOY corresponding to the back projected locations of the

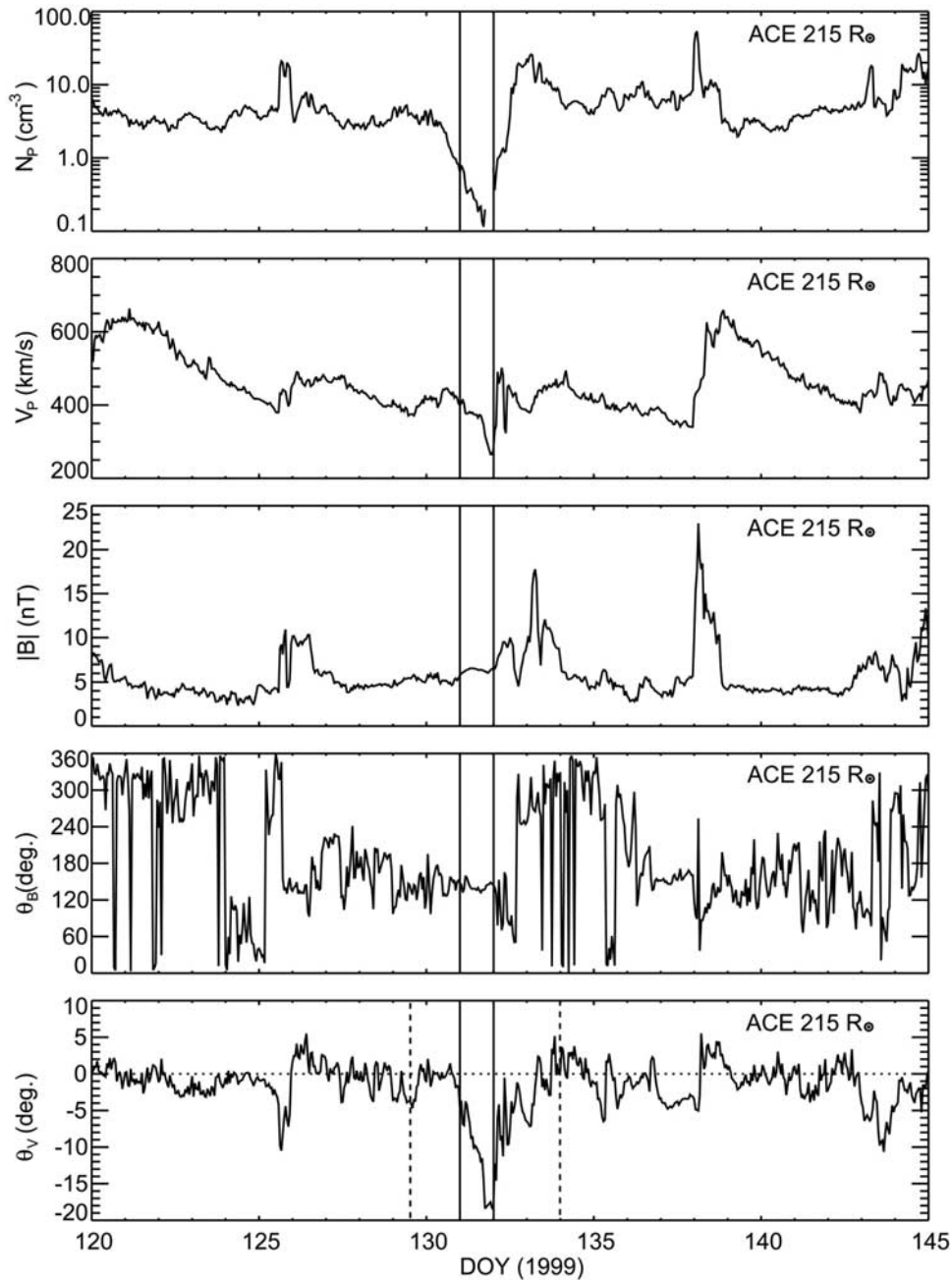


Figure 2. Shown starting from the top and plotted as a function of day number in 1999 are ACE in situ measurements at 1 AU of proton density, proton velocity, magnitude of the IMF, azimuthal direction of the magnetic field in the ecliptic plane, and the deviation, in degrees, of the solar wind flow from the radial direction, respectively. The solid parallel lines running vertically across all parts demarcate DOY 131 when the disappearance event took place. The dashed parallel lines running vertically across the lowermost part are drawn at DOY 129.5 and 134 when the solar wind flow direction returned to being radial after the disappearance event.

observed ACE spacecraft velocities at 1 AU on DOY 131. It can be seen from Figure 4 (uppermost part) that the transient low-velocity, low-density flows observed at 1 AU on DOY 131 originated on the Sun at heliographic longitudes between $\sim 280^\circ$ and 300° . The dashed parallel lines running vertically across both the parts bracket the traceback locations of DOY 129.5 and DOY 134 when the solar wind flow returned to being radial after showing large

deviations from the radial flow directions between DOY 131 and 132.

3.2.1. Origin of Nonradial Flows and Estimation of Source Location

[11] In the solar corona where the plasma beta ($\beta = 2nkT/[B^2/8\pi]$) is low coronal mass flows upward along open magnetic field to become the solar wind, and as β increases this solar wind drags the field out into the well-known

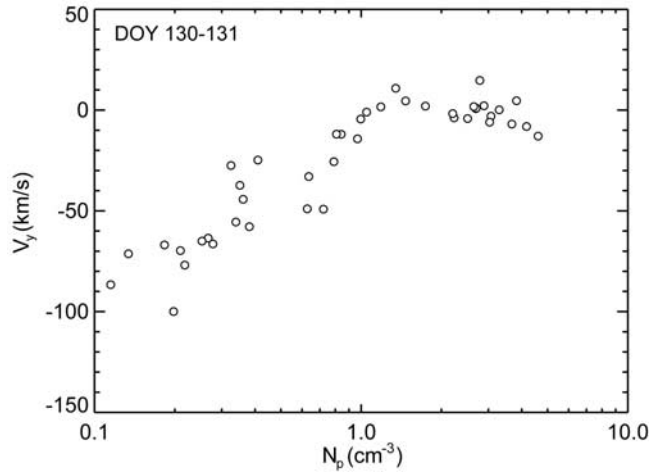


Figure 3. Shows a plot of the variation of density as a function of the azimuthal component (V_y) of the solar wind velocity on DOY 130–131.

Parker spiral. The radial distance at which this happens will depend upon physical conditions of density and magnetic field intensity and is referred to as the Alfvén radius (R_A) which normally extends only out to 0.05 AU or $\sim 10 R_\odot$. However, ACE measurements have shown that the deviations from radial flow of the solar wind on DOY 131 was such that the azimuthal component of the solar wind velocity (V_a), in GSE coordinates, went as high as 100 km s^{-1} . It may be noted here that the magnetic field intensity remained unchanged during the low-density event. This would imply that the Alfvén radius would be mainly determined by the density and not by the magnetic field. This can also be inferred from Figure 3 which shows a strong inverse correlation between the azimuthal velocity and the density. Another point to be noted is that the variance of the magnetic field intensity is low and the field direction is in the expected Parker spiral direction. This strongly suggests that the low-density flow was a corotating stream. If we therefore assume that this azimuthal velocity component was due to corotation of the solar wind out to a distance R_A , then R_A could extend out 0.23 AU or $\sim 50 R_\odot$ since $R_A \Omega_\odot = V_a$, where the Sun’s angular speed $\Omega_\odot = 1.642 \times$

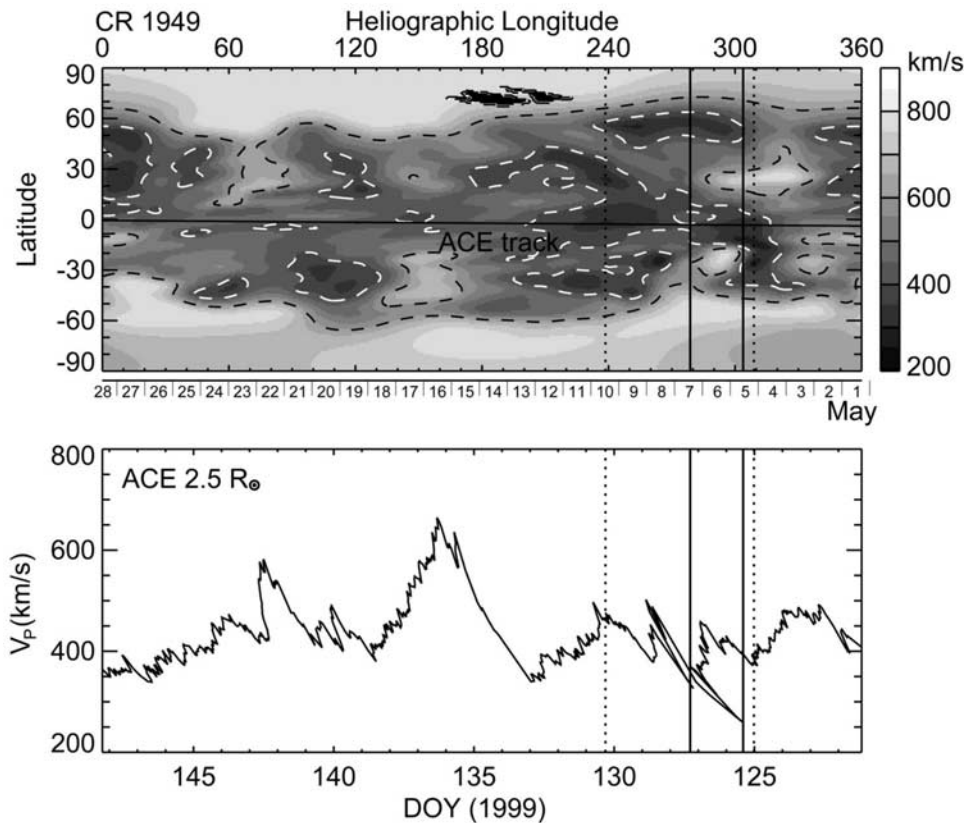


Figure 4. (top) A tomographic synoptic velocity map projected on the source surface at $2.5 R_\odot$ for CR1949 in May 1999, obtained using STEL IPS data. The dashed white and black lines demarcate respectively, the boundaries of the low-velocity flows ($< 400 \text{ km s}^{-1}$), and polar coronal hole boundaries. Dates of CMP are indicated at the bottom of the map with the corresponding heliographic longitudes marked at the top of the map. The path of the ACE spacecraft is indicated by a thick line along the equator. (bottom) ACE in situ measurements of proton velocities that have been mapped back along Archimedean spirals to the source surface at $2.5 R_\odot$. The solid and dashed vertical parallel lines in both parts correspond to the traced back locations of the corresponding lines in Figure 2.

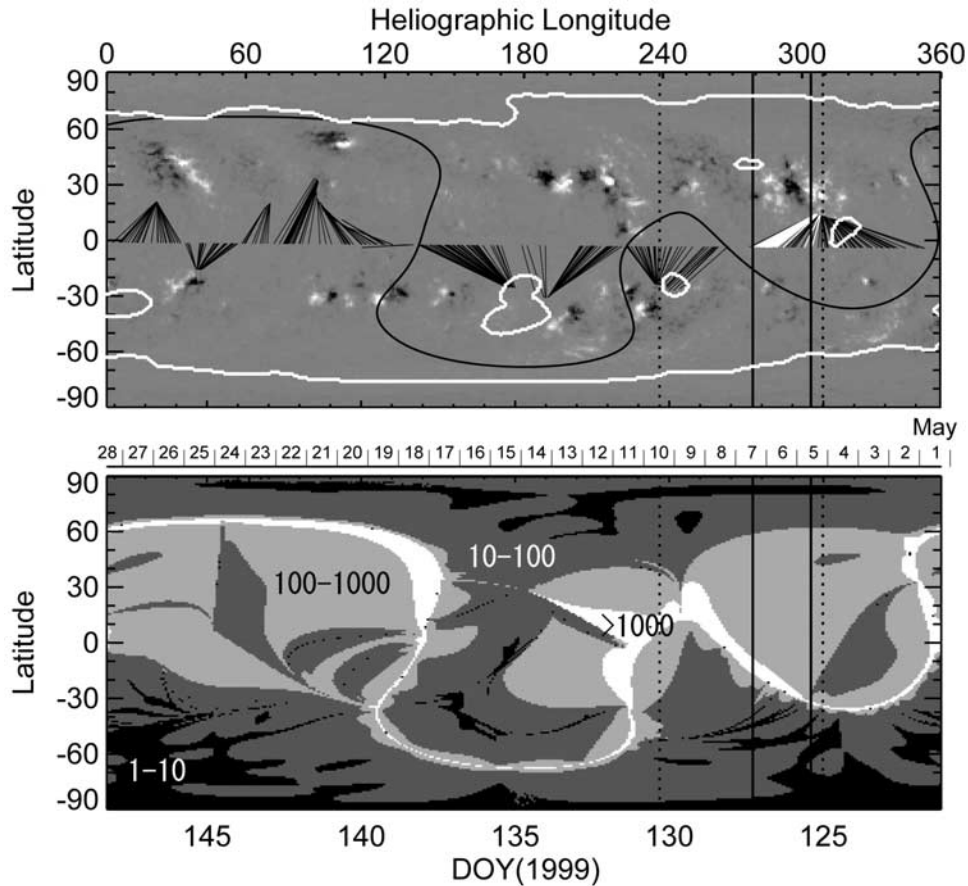


Figure 6. (top) A synoptic map for CR1949 in May 1999 made using magnetograms from the MDI instrument on board SOHO. Heliographic longitude is marked at the top, while CMP dates are marked at the bottom of the map. Regions of large magnetic field strength corresponding to active region locations are shown as black and white patches to distinguish the two magnetic polarities. The curved solid line is the magnetic neutral line. Converging black lines on the map join magnetic fields on the source surface at $2.5 R_{\odot}$, derived from potential field computations, with their corresponding counterparts on the photosphere. The potential field lines that are marked in white correspond to fields with CMP date of 11 May 1999. Also shown by thick white lines are the locations of CH boundaries inferred from HeI 10830Å observations. (bottom) A map of the magnetic flux expansion rates with the white, light grey, dark grey, and black regions corresponding to flux expansion rates of >1000 , between 100 and 1000, between 10 and 100, and between 1 and 10, respectively. The two sets of solid and dashed vertical parallel lines demarcate the back projected location of DOY 131 when the solar wind flow was nonradial and days on either side of DOY 131 when the solar wind flow was radial, respectively.

[14] Overplotted on the synoptic map and shown by thick white lines are the locations of the coronal hole boundaries during CR 1949 determined from HeI 10830Å observations from Kitt Peak. Note the location of the small coronal hole lying very close to the converging potential field lines that are shown in white. It can therefore be argued from Figure 6 (top) that the tenuous solar wind flows at 1 AU during DOY 131 probably originated from this coronal hole on the Sun and in the vicinity of the large active region, identified as AR8525, lying at $\sim 18^{\circ}$ N and between heliographic longitudes 280° and 300° . The lower part of Figure 6 shows a map of the magnetic flux expansion rates. The white regions indicate locations with expansions factors >1000 , while the light grey, dark grey, and black regions indicate regions with flux expansion factors in the ranges 100–1000, 10–100, and 1–10, respectively. The flux expansion rate is given by

$S_x = \frac{B_{ps}}{B_{ss}} \times \left(\frac{R_{\odot}}{2.5 \times R_{\odot}}\right)^2$, where B_{ps} and B_{ss} are the radial components of the magnetic field, derived from potential field computations, at the photosphere and at the source surface at $2.5 R_{\odot}$ respectively.

3.3.1. Low-Speed Solar Wind Flows

[15] Unlike high-speed solar wind that emanates only from large open field regions called coronal holes, the low-speed solar wind can have different origins. Low-speed solar wind outflows are known to emanate from the tops of closed coronal loops in helmet streamers and from the outer boundaries of closed loop regions in active regions [Wang *et al.*, 1998]. A high correlation has also been found between solar wind speed and the size of the coronal hole from which it originates [Nolte *et al.*, 1976; Wang and Sheeley, 1990; Neugebauer, 1994; Wang, 1994; Neugebauer *et al.*, 1998; Kojima *et al.*, 1999]. A recent study [Ohmi *et al.*,

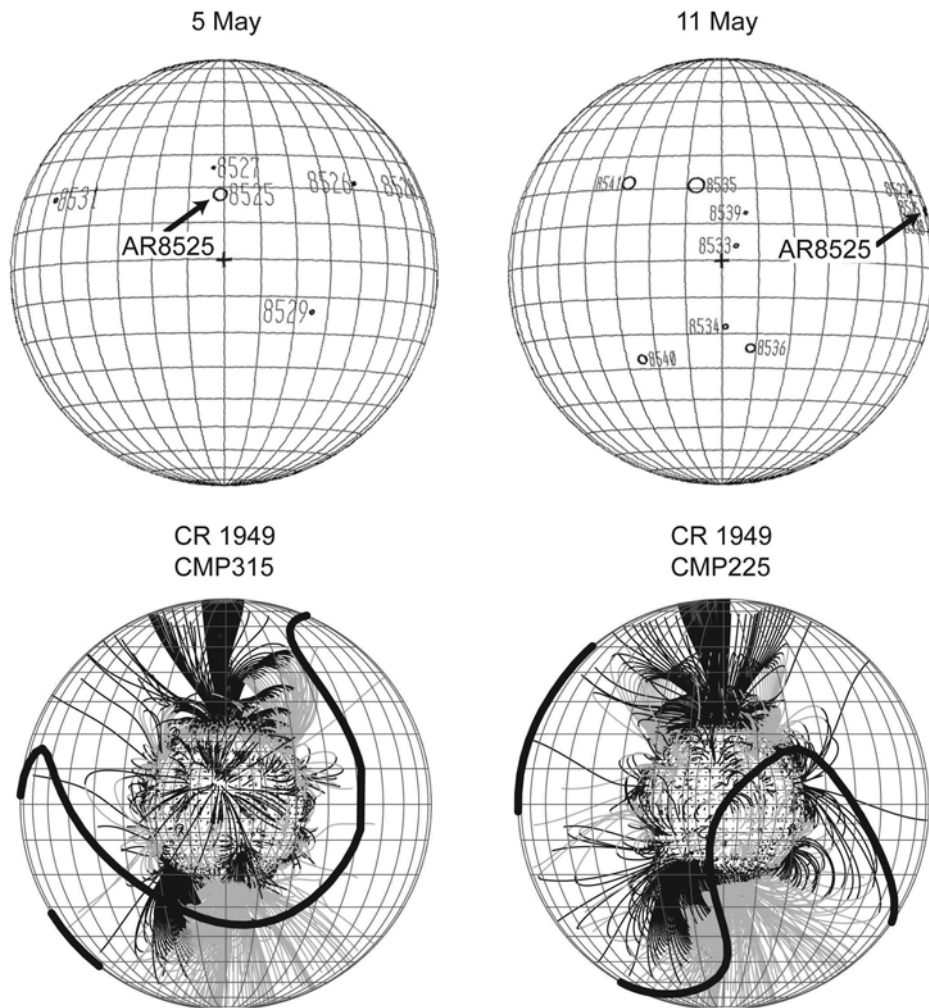


Figure 7. Maps of the solar photosphere on 5 May and 11 May 1999 are shown in the upper left and right-hand parts, respectively, indicating the locations of the large active regions. The location of AR8525 is indicated by an arrow in both the upper parts. The lower two parts show the three-dimensional structure of the coronal magnetic fields for CR1949 on 5 May 1999 (left-hand part) and 11 May 1999 (right-hand part). The fields were computed using a potential field model and are viewed from 315° (left) and 225° (right) in Carrington longitude. The black and grey lines denote the outward and inward polarities, respectively, and are shown projected on to the source surface at $2.5 R_\odot$. Only fields between 5 G and 250 G on the photosphere are plotted in order not to clutter the figure. The open field lines at $2.5 R_\odot$ are plotted in steps of 5° in longitude and latitude. The thick curved line in the lower two parts is the magnetic neutral line.

2003] has shown that polar coronal holes, normally sources of very fast wind, can turn into sources of very slow solar wind with outflow velocities slower than the mean expected solar wind values. This happens when the polar coronal holes undergo an enormous reduction in size and area, during solar maximum, before finally disappearing altogether.

[16] It has also been shown that solar wind speeds are inversely correlated with the expansion factors of magnetic flux tubes, with lower speeds coming from regions having large magnetic flux expansion factors [Wang and Sheeley, 1990, 1991; Sheeley *et al.*, 1991] and vice versa. It is clear from the second part of Figure 6 that apart from locations tracing the magnetic neutral line, which are expected to have large flux expansion factors, there are other large regions with high flux expansion factors covering the source surface. This supports the evidence from the tomographic

synoptic map (Figure 3, top) that large portions of the inner heliosphere during CR 1949 in May 1999 were dominated by stable low velocity flows.

4. Active Regions Locations

[17] The upper two parts of Figure 7 show maps of the solar photosphere indicating the locations of the large active regions on 5 May 1999 (upper left part) and 11 May 1999 (upper right part) with the location of AR8525 shown by an arrow. The lower two parts in Figure 7 show the three-dimensional structure of the coronal magnetic field for CR1949 on DOY 125 (lower left part) and DOY 131 (lower right part). It is important to bear in mind here that the CMP date of 11 May 1999 corresponds to a longitude of 225° . The lower right part is therefore shown as viewed from a

Carrington longitude of 225° , while the lower left part is shown as viewed from a Carrington longitude of 315° corresponding to a CMP date of 5 May 1999. The differently shaded magnetic field lines distinguish the two polarities and are shown projected on to a source surface at $2.5 R_\odot$ beyond which the potential field lines are assumed to be radial. The black field lines are the outward or positive polarity lines, while the grey field lines correspond to inward or negative polarity. Only fields between 5 G and 250 G on the photosphere are plotted. The thick wavy line in the lower two parts is the magnetic neutral line. In the upper two parts, it is important to note that the large active region AR8525 was at central meridian on DOY 125 (5 May 1999) and on the west limb on DOY 131 (11 May 1999). It is clear from the lower two parts of Figure 7 that the open field lines seen fanning out into the interplanetary medium from the west limb (lower right part) and from central meridian (lower left part) originate from the location of the large active region complex of which AR8525 is a part. It should be noted that apart from this large open field structure, whose central meridian location on DOY 125 would have produced Earth-directed outflows, the midlatitudes in both hemispheres are entirely dominated by closed loop structures. In other words, the potential field computations have not revealed any other open field configurations on the photosphere.

5. Possible Solar Source of the Low-Velocity, Low-Density Flows: A Small Coronal Hole

[18] It is known that many midlatitude and equatorial coronal holes are located on the trailing edge of active regions [Balogh *et al.*, 1995]. Our study shows that the low-velocity, low-density solar wind observed during the disappearance event may have originated in the vicinity of an active region AR8525 located at central meridian on DOY 125 around 18°N and between heliographic longitudes 280° and 300° . The location of a small coronal hole very close to AR8525 and to its southwest (see Figure 6) indicates that it was possibly the source of the tenuous solar wind flows of 11 May 1999. It is important to bear in mind that the central meridian location of AR8525 on DOY 125 would imply that the flows from this region would have been Earth-directed. Also, the IMF during DOY 131–132 was stable (showing a very low variance) and unipolar. If the small coronal hole (seen in Figure 6) were indeed the source of the tenuous flows of 11 May 1999 then the low velocities observed could be easily explained, as described earlier in section 3.3.1, as a consequence of the small size of the coronal hole and the large magnetic flux expansion factors from the region.

[19] One method of producing the low densities would be by assuming that rearrangements in CH boundaries would produce a pinch-off or separation of the solar wind outflow, thereby completely detaching the outflow from its solar source. Since coronal hole boundaries locate separatrices of coronal magnetic fields, which in turn are continuously evolving, the boundaries of coronal holes are constantly changing and evolving. Thus it is entirely possible that changes in the CH boundaries could lead to a pinch-off or separation in the solar wind outflow, especially if the CH were small in size. If such a detached outflow occurred

within ~ 48 hours of its start and it continued to expand as it propagated out to 1 AU, then it can be argued that an increase in its radius by a factor of 6–7 would lead to a decrease in densities by a factor of ~ 200 – 300 at 1 AU. Thereby, typical particle densities of approximately 20 – 30 particles cm^{-3} at 0.5 AU could be reduced to 0.1 particles cm^{-3} at 1 AU given that the typical travel time between the Sun and the Earth, at these low velocities, is ~ 5 days. Thus simple expansion of this large, detached, low-velocity flow region, as it propagated out to 1 AU, could give rise to an extremely low-density cloud that engulfed the Earth as observed on DOY 131.

6. Discussion and Conclusion

[20] White light observations from the LASCO coronagraphs during May 1999 have shown that the solar corona was unusually quiet for a period around the maximum with no large CMEs taking place during the entire week preceding the disappearance event. We can therefore say that the large, low-density, low-velocity cloud that engulfed the Earth on 11 May 1999 was not associated with an interplanetary CME. A. V. Usmanov (private communication, 2003) searched the OMNI and ACE spacecraft databases from 1963 onward and found seven cases of dramatic density depletions (with densities less than 1 cm^{-3}). Four of these events have occurred close to the solar maximum, while the remaining have occurred well within 2 years of the maximum when solar activity was still high. The most dramatic of these seven events was the long-duration density depletion in the interplanetary medium [Schwenn, 1983; Gosling *et al.*, 1982] observed by Helios1 and Helios2 spacecraft that occurred in November 1979 and June 1980 during solar maximum in cycle 21. The fact that June 1980 in solar cycle 21 and May 1999 in solar cycle 23 both corresponded to periods during which solar polar field reversals were taking place led to speculation [Balasubramanian *et al.*, 2003] that the large-scale restructuring of the solar magnetic fields during solar polar field reversals is likely to be associated with density anomalies. The current work indicates that the connection of such events with polar field reversal periods is incidental in that the solar maximum period is dominated by large active regions and a highly deformed neutral line configuration, thereby maximizing the likelihood for the formation of small TCH [Kahler and Hudson, 2001] and/or small midlatitude CH. Also, midlatitude and equatorial coronal holes are nearly absent during the solar minimum phase, thereby increasing the likelihood of such events being observed only at or around solar maximum. It must also be borne in mind that spacecraft observations are confined to the ecliptic, another reason for observing such events at or around solar maximum because of the increased probability for the occurrence of midlatitude and equatorial coronal holes during solar maximum.

[21] Using IPS observations along with in situ ACE data, MDI magnetograms and Hel 10830Å observations during CR1949 we have been able to locate with a reasonable degree of accuracy the solar source of the May 1999 solar wind disappearance event. We have shown that the large azimuthal velocities observed during the event would not produce very serious errors in the source locations determined by the constant velocity traceback technique. Our

observations strongly suggest that the low-velocity flows came from a small positive-polarity region at the east end of a large bipolar magnetic region on the Sun located in the vicinity of the large active region AR8525 that was at central meridian and lying close to the highly deformed magnetic neutral line on 5 May 1999. In addition, potential field computations of the source surface magnetic fields were used to show that the only large open magnetic field configuration on the photosphere originated from the location of the large active region complex of which AR8525 is a part. Using Hel 10830A observations of CH boundaries, we located a small CH very close to this source location and concluded that this small, midlatitude CH was most probably the source of the low-velocity flows of 11 May 1999. A mechanism for producing the low densities observed at 1 AU on 11 May 1999 was then suggested.

[22] The appropriately located small CH during CR1949, the location of AR8525 at central meridian on DOY 125, and the large flux expansion factors (see Figure 6) would imply that the solar wind emanating from this region would be Earth-directed and have low velocities, taking ~ 5 days to cover the Sun-Earth distance of 1 AU at an average velocity of ~ 350 km s $^{-1}$. In addition, as stated in section 3.3.1, low-speed wind emanating from small coronal holes are always associated with large flux expansion factors. The densities in such low-velocity flows are, however, not abnormally low. However, since midlatitude CH boundaries are constantly undergoing change, it is possible that some sort of pinch-off could occur and lead to a large detached flow region into the interplanetary medium. Expansion of this large flow region as it propagated outward could then give rise to the extremely low densities that engulfed the Earth on DOY 131, as explained earlier. Finally, it has been suggested in an earlier work [Balasubramanian et al., 2003] that the morphology of the void that engulfed the Earth and caused the disappearance event was that of a void-in-void. It is possible that the inner void could have been caused by the detached and expanding outflow from the CH, while the outer void represents the steady low-velocity background from the small CH as indicated by the large open field region seen in the lower two parts of Figure 7.

[23] The present work, by identifying a localized solar source on the Sun for the origin of low-velocity, low-density flows during the “disappearance event,” suggests that the association of such events with global, large-scale solar phenomena like the periodic 11-year solar polar field reversal, as has been suggested by Usmanov et al. [2000] and Balasubramanian et al. [2003], is most likely to be coincidental. More observations of such events will be required before this can be stated with statistical confidence. While the small area of the source location and large flux expansion factors seen from the region explain the low velocities observed [Wang and Sheeley, 1990; Sheeley et al., 1991; Nolte et al., 1976; Neugebauer et al., 1998], the observed low densities can be explained by the outward expansion of the detached low-velocity cloud as it propagated out to 1 AU. As stated earlier, since coronal hole boundaries locate separatrixes of coronal magnetic fields, which in turn define its large-scale current systems, this work has also highlighted the need for systematic studies of the dynamics and evolution of CH boundaries. Such studies

could help define coronal hole boundary structure and help in understanding boundary field connectivities. We believe that regular and systematic observations by both ground and space based platforms will be required to identify many more such events and ground-based IPS observations can play an important role in such future studies.

[24] **Acknowledgments.** The authors would like to thank the anonymous referees for their constructive comments that have gone a long way in making this paper much clearer. The authors also thank the ACE SWEPAM instrument team and the ACE Science Center for making ACE Level 2 data available in the public domain via the World Wide Web. One of the authors, P. Janardhan, would like to thank Murray Dryer, NOAA, Boulder, Colorado, USA for very useful suggestions and to acknowledge support provided by a 3-month visiting position during 2003, at the Solar-Terrestrial Environment Laboratory, Toyokawa, Japan during which this work was carried out. The work by Fujiki, Kojima, and Tokumaru was partially supported by the Japan Society for the Promotion of Sciences (grants 12440130, 15340162).

[25] Shadia Rifai Habbal thanks Adam Rees, Neil R. Sheeley Jr., and another referee for their assistance in evaluating this paper.

References

- Asai, K., M. Kojima, M. Tokumaru, A. Yokobe, B. V. Jackson, P. L. Hick, and P. K. Manoharan (1998), Heliospheric tomography using interplanetary scintillation observations: 3. Correlation between speed and electron density fluctuations in the solar wind, *J. Geophys. Res.*, *103*, 1991–2001.
- Balasubramanian, V., P. Janardhan, S. Srinivasan, and S. Ananthakrishnan (2003), IPS observations of the solar wind disappearance event of May 1999, *J. Geophys. Res.*, *108*(A3), 1121, doi:10.1029/2002JA009516.
- Balogh, A. J., A. Gonzalez-Esparza, J. A., R. J. Forsyth, M. E. Burton, B. E. Goldstein, E. J. Smith, and S. J. Bame (1995), Interplanetary shock waves: Ulysses observations in and out of the ecliptic plane, *Space Sci. Rev.*, *72*, 171–180.
- Burlaga, L. F. (1974), Interplanetary stream interfaces, *J. Geophys. Res.*, *79*, 3717–3725.
- Crooker, N. U., S. Shodhan, J. T. Gosling, J. Simmerer, R. P. Lepping, J. T. Steinberg, and S. W. Kahler (2000), Density extremes in the solar wind, *Geophys. Res. Lett.*, *27*, 3769–3772.
- Farrugia, C. J., H. J. Singer, D. Evans, D. Berdichevsky, J. D. Scudder, K. W. Ogilvie, R. J. Fitzenreiter, and C. T. Russell (2000), Response of the equatorial and polar magnetosphere to the very tenuous solar wind on May 11, 1999, *Geophys. Res. Lett.*, *27*, 3773–3776.
- Gosling, J. T., J. R. Asbridge, S. J. Bame, and W. C. Feldman (1978), Solar wind stream interfaces, *J. Geophys. Res.*, *83*, 1401–1412.
- Gosling, J. T., J. R. Asbridge, S. J. Bame, W. C. Feldman, R. G. Zwickl, G. Pashmann, N. Sckopke, and C. T. Russell (1982), A sub-alfvénic solar wind: interplanetary and magnetosheath observations, *J. Geophys. Res.*, *87*, 239–245.
- Hakamada, K., and M. Kojima (1999), Solar wind speed and expansion rate of the coronal magnetic field during carrington rotation 1909, *Sol. Phys.*, *187*, 115–122.
- Jackson, B. V., P. L. Hick, M. Kojima, and A. Yokobe (1998), Heliospheric tomography using interplanetary scintillation observations: 1. Combined Nagoya and Cambridge data, *J. Geophys. Res.*, *103*, 12,049–12,068.
- Janardhan, P., V. Balasubramanian, S. Ananthakrishnan, M. Dryer, A. Bhatnagar, and P. S. McIntosh (1996), Traveling interplanetary disturbances detected using interplanetary scintillation at 327 MHz, *Sol. Phys.*, *166*, 379.
- Kahler, S. W., and H. S. Hudson (2001), Origin and development of transient coronal holes, *J. Geophys. Res.*, *106*, 29,239–29,248.
- Kakinuma, T., and M. Kojima (1984), Three-station observations of interplanetary scintillation at 327 MHz 1, *Proc. Res. Inst. Atmos.*, *31*, 1–4.
- Kojima, M., M. Tokumaru, H. Watanabe, A. Yokobe, K. Asai, B. V. Jackson, and P. L. Hick (1998), Heliospheric tomography using interplanetary scintillation observations II latitude and heliocentric distance dependence of solar wind structure, *J. Geophys. Res.*, *103*, 1981–1989.
- Kojima, M., K. Fujiki, M. Ohmi, M. Tokumaru, A. Yokobe, and K. Hakamada (1999), Low speed solar wind from the vicinity of solar active regions, *J. Geophys. Res.*, *104*, 16,993–17,003.
- Neugebauer, M. (1994), Observation of the solar wind from coronal holes, *Space Sci. Rev.*, *70*, 319–330.
- Neugebauer, M., et al. (1998), Spatial structure of the solar wind and comparisons with solar data and models, *J. Geophys. Res.*, *103*, 14,587–14,600.
- Nolte, J. T., A. S. Krieger, A. F. Timothy, R. E. Gold, E. C. Roelof, G. Vaiana, A. J. Lazarus, J. D. Sullivan, and P. S. McIntosh (1976), Coronal holes as sources of solar wind, *Sol. Phys.*, *46*, 303–322.

- Ohmi, T., M. Kojima, K. Fujiki, M. Tokumaru, and K. Hayashi (2003), Polar low-speed solar wind reappeared at the solar activity maximum of cycle 23, *Geophys. Res. Lett.*, *30*(7), 1409, doi:10.1029/2002GL016347.
- Richardson, I. G., D. Berdichevsky, M. D. Desch, and G. J. Farrugia (2000), Solar-cycle variation of low density solar wind during more than 3 solar cycles, *Geophys. Res. Lett.*, *27*, 3761–3764.
- Schwenn, R. (1983), The average solar wind in the inner heliosphere: Structure and slow variations, *Solar Wind 5*, edited by M. Neugebauer, *NASA Conf. Publ.*, CP-2280, 489–508.
- Sheeley, N. R., Jr., E. T. Swanson, and Y.-M. Wang (1991), Out of the ecliptic tests of the inverse correlation between solar wind speed and coronal expansion factor, *J. Geophys. Res.*, *96*, 13,861–13,868.
- Usmanov, A. V., M. L. Goldstien, and W. M. Farrell (2000), A view of the inner heliosphere during the May 10–11, 1999 low density anomaly, *Geophys. Res. Lett.*, *27*, 3765–3768.
- Vats, H. O., H. S. Sawant, R. Oza, K. N. Iyer, and R. Jadhav (2001), Interplanetary scintillation observations of the solar wind disappearance event of May 1999, *J. Geophys. Res.*, *106*, 25,121–25,124.
- Wang, Y.-M. (1994), Two types of solar wind, *Astrophys. J.*, *437*, L67–L70.
- Wang, Y.-M., and N. R. Sheeley Jr. (1990), Solar wind speed and coronal flux-tube expansion, *Astrophys. J.*, *355*, 726–732.
- Wang, Y.-M., and N. R. Sheeley Jr. (1991), Why fast solar wind originates from slowly expanding coronal flux tubes, *Astrophys. J.*, *372*, L45–L48.
- Wang, Y.-M., N. R. Sheeley Jr., J. H. Walters, G. E. Brukner, R. A. Howard, D. J. Michels, P. L. Lamy, R. Schwenn, and G. M. Simnett (1998), Origin of streamer material in the outer corona, *Astrophys. J.*, *498*, L165–L168.
-
- K. Fujiki, K. Kojima, and M. Tokumaru, Solar-Terrestrial Environment Laboratory, Nagoya University, Honohara 3-13, Toyokawa, Aichi, 442-8507, Japan. (fujiki@stelab.nagoya-u.ac.jp; kojima@stelab.nagoya-u.ac.jp; tokumaru@stelab.nagoya-u.ac.jp)
- K. Hakamada, Department of Natural Science and Mathematics, Chubu University, 1200 Matsumoto-cho, Kasugai 487-8501, Japan. (hakamada@solan.chubu.ac.jp)
- P. Janardhan, Astronomy and Astrophysics Division, Physical Research Laboratory, Ahmedabad 380 009, India. (jerry@prl.ernet.in)